Eur. Phys. J. E (2014) **37**: 87
DOI 10.1140/epje/i2014-14087-0

THE EUROPEAN PHYSICAL JOURNAL E

Regular Article

The influence of nanoparticle migration on forced convective heat transfer of nanofluid under heating and cooling regimes*

Sofya V. Kozlova[a] and Ilya I. Ryzhkov

Institute of Computational Modelling SB RAS, Akademgorodok, 50/44, 660036 Krasnoyarsk, Russia

Received 2 July 2014 and Received in final form 30 July 2014
Published online: 30 September 2014 –

Abstract. In this paper, laminar convective heat transfer of water-alumina nanofluid in a circular tube with uniform heat flux at the tube wall is investigated. The investigation is performed numerically on the basis of two-component model, which takes into account nanoparticle transport by diffusion and thermophoresis. Two thermal regimes at the tube wall, heating and cooling, are considered and the influence of nanoparticle migration on the heat transfer is analyzed comparatively. The intensity of thermophoresis is characterized by a new empirical model for thermophoretic mobility. It is shown that the nanoparticle volume fraction decreases (increases) in the boundary layer near the wall under heating (cooling) due to thermophoresis. The corresponding variations of nanofluid properties and flow characteristics are presented and discussed. The intensity of heat transfer for the model with thermophoresis in comparison to the model without thermophoresis is studied by plotting the dependence of the heat transfer coefficient on the Peclet number. The effectiveness of water-alumina nanofluid is analyzed by plotting the average heat transfer coefficient against the required pumping power. The analysis of the results reveals that the water-alumina nanofluid shows better performance in the heating regime than in the cooling regime due to thermophoretic effect.

1 Introduction

Nanofluids are colloidal suspensions consisting of base fluid and nano-sized particles. The particles are typically made of oxides, metals, and carbon nanotubes. Liquids used as base fluids are commonly water, ethylene glycol, and oil. The presence of a small amount of nanoparticles in the base fluid enhances its thermal conductivity. In this way, nanofluids can potentially be used as heat transfer fluids for cooling electronic devices, vehicle engines, nuclear reactors, laser diodes, etc. [1]. But the addition of nanoparticles leads to a viscosity increase of the base fluid. The effectiveness of nanofluids in forced convective heat transfer depends on whether the thermal conductivity enhancement can override the penalty in pumping power associated with the viscosity increase [2]. The production of stable nanofluids with prescribed physical properties for commercial use still remains a challenging problem [3].

The use of nanofluids requires a clear understanding of heat transfer mechanisms, which contribute to their enhanced thermal properties. Contradictions between results measured by different authors (see review [4]) promoted the development of theoretical concepts for heat transfer in nanofluids. Several potential mechanisms were suggested: Brownian motion of nanoparticles, formation of highly conductive liquid nanolayer at the liquid-particle interface, nanoparticle clustering, ballistic transfer of heat energy inside a separate nanoparticle and between nanoparticles upon contact, dispersion of nanoparticles, and thermophoresis (nanoparticle transport driven by temperature gradient) [5–7]. However, the contribution of these mechanisms to the effective thermal conductivity of nanofluids is not fully understood.

There exist different approaches to describe the flow and heat transfer in nanofluids. One of them is *the homogeneous one-component model*, based on the momentum and heat transfer equations with physical properties corresponding to nanofluids. It implies that the traditional heat transfer correlations must be valid for nanofluids [3]. The second approach is suggested by Buongiorno [8]. It is known as *non-homogeneous two-component model* which treats nanofluid as a mixture of the base fluid and nanoparticles. The system is described by the equations of momentum, heat and nanoparticle transfer. According to [8], Brownian diffusion and thermophoresis are the main mechanisms that induce variations of nanoparticle concentration. In general, further studies are needed to verify the existing models of nanofluids.

A large amount of experimental data on convective heat transfer in nanofluids can be found in the literature. In most studies, nanofluids are pumped through a circular tube with uniform heat flux at the wall. The exten-

* Contribution to the Topical Issue "Thermal non-equilibrium phenomena in multi-component fluids" edited by Fabrizio Croccolo and Henri Bataller.

[a] e-mail: sonique@icm.krasn.ru

sive reviews are presented in papers by Yu *et al.* [9] and Terekhov *et al.* [10]. The enhancement of heat transfer coefficient with respect to base fluids is reported to be from a few percents for oxide nanoparticles up to 350% for carbon nanotubes [11]. In some studies, the measured Nusselt numbers followed classical heat transfer correlations such as Shah correlation for laminar flows and Dittus-Boelter correlation for turbulent flows as well as their modifications for temperature-dependent physical properties [12–15]. Experimental measurement of heat transfer coefficient for water-copper oxide nanofluid in a cylindrical channel was presented by Guzei *et al.* in [16]. The nanofluid appeared to be non-Newtonian when particle concentration exceeded 0.25%. Some experimental results for water-alumina nanofluid showed anomalous heat transfer enhancement in laminar regime [17,18]. The conjectured reasons of this enhancement were particle migration due to non-uniform shear rate, viscosity gradient, or thermophoretic migration of nanoparticles. Measurements of the Nusselt number for water-Cu nanofluid in turbulent regime [19] provided a 30% increase in comparison with the Dittus-Boelter correlation for 2% volume fraction of nanoparticles. These results cannot be explained on the basis of a homogeneous flow model. Numerical simulation of turbulent convection in water-alumina nanofluid in a cylindrical tube with constant wall temperature was presented in [20]. It was found that heat transfer was enhanced with increasing nanoparticle volume fraction. The latter was accompanied by the increase of wall shear stress. In most studies, comparison between heat transfer coefficients of the base fluids and nanofluids was made at the same Reynolds number. Yu *et al.* [2] and Utomo *et al.* [14] showed that this method distorts the physical situation since nanofluids require a higher average velocity than the base fluids to achieve the same Reynolds number due to viscosity increase. From an engineering point of view, the comparison must be performed at the same pumping power, which determines the cost of transferring the heat.

The effect of particle migration on convective heat transfer of nanofluids in a laminar regime has been studied in a number of works. Wen and Ding [21] considered three mechanisms leading to non-uniform concentration of particles in the radial direction: non-uniform shear rate, viscosity gradient, and Brownian diffusion. This study was continued in [22], where a numerical simulation on the basis of a combined Euler and Lagrange approach was performed. Using the order-of-magnitude analysis, Sohn and Kihm [23] showed that thermophoresis and Brownian diffusion are the most important mechanisms of particle migration, while the effects of viscosity gradient and non-uniform shear rate can be neglected. Numerical simulations on the basis of a homogeneous model showed that the Nusselt number for laminar flow is independent of nanoparticle concentration. When the non-homogeneous model is used, the Nusselt number increases (decreases) with increasing nanoparticle concentration when the tube wall is heated (cooled). Na *et al.* [24,25] investigated laminar convective heat transfer in water-alumina nanofluid. They found that the dynamic thermal conductivity of nanofluid increases (decreases) with increasing the Reynolds number in the wall heating (cooling) regime. It was attributed to the thermophoretic migration of nanoparticles. However, the dynamic thermal conductivity was calculated either from both experimental and numerical data [24] or under the assumption of fully developed temperature profile [25]. Thus, the entrance region that can be rather large for high Reynolds numbers was neglected. Numerical and experimental study of convective heat transfer in water-TiO_2 nanofluid was performed in [26]. It was argued that taking particle migration into account provides better agreement between experimental and numerical values of heat transfer coefficient.

The theoretical models considered in [21,23–26] do not take convective transport of nanoparticles into account. It leads to essentially non-uniform concentration profile in the tube cross-section, which is not differentiable near the centerline. Heyhat and Kowsary [27] performed numerical simulation of convective heat transfer in water-alumina nanofluid on the basis of a non-homogeneous model taking into account convective transport of nanoparticles. Constant temperature was maintained on the tube wall. They showed that thermophoresis reduces nanoparticle concentration only in the wall boundary layer. The corresponding viscosity reduction leads to the increase of velocity near the wall. At the tube center, the velocity profile is flattened in order to keep the mass flow rate constant. The heat transfer coefficient was shown to increase in comparison with homogeneous model prediction. In particular, the increase was around 8% for 5% volume fraction of nanoparticles. The analytical solution for temperature and nanoparticle volume fraction in the tube with Poiseuille flow and constant wall heat flux was recently obtained by Ryzhkov [28]. It confirmed that thermophoretic separation is limited to the wall boundary layer.

To describe thermophoresis in nanofluids, Buongiorno [8] suggested to use the formula for thermophoretic velocity that was originally derived for rigid particles in gases [29] and later corrected for liquids on the basis of experimental data [30]. According to this formula, the thermophoretic velocity is proportional to the fluid viscosity. However, a vast majority of theoretical and experimental results [31,32] as well as molecular dynamics simulations [33] suggest that thermophoretic velocity in colloidal suspensions is inversely proportional to the fluid viscosity. A consistent empirical model for thermophoretic mobility was suggested on the basis of experimental data and theorerical concepts by Ryzhkov and Minakov in [34]. It was stated that the thermophoretic mobility is proportional to the thermal expansion coefficient of the solvent and inversely proportional to its viscosity. The investigation of heat and nanoparticle transfer in a circular tube heated with a constant heat flux was performed.

The presented literature review shows that further studies are needed to understand the effect of thermophoresis on heat transfer in nanofluids. In this paper, we perform a numerical study of laminar convective heat transfer of water-alumina nanofluid in a circular tube with uniform heat flux at the tube wall. Two thermal

regimes are considered, heating and cooling. The physical properties of nanofluid are taken from experimental measurements. A generalization of non-homogeneous two-component model to the case of compressible flow is used for calculations. The effects of Brownian diffusion, thermophoresis, and variable physical properties on the velocity, temperature, and nanoparticle volume fraction fields are investigated. The comparative analysis of heat transfer in each thermal regime is accomplished by several heat transfer characteristics.

The paper is organized as follows. In sect. 2, the physical properties of water-alumina nanofluid are described. In sect. 3, the flow geometry, governing equations, physical parameters, and solution methods are provided. The results of calculations are presented and discussed in sect. 4.

2 Thermophysical properties of water-alumina nanofluid

The physical properties of water-alumina nanofluid depend on the properties of water and alumina nanoparticles as well as nanoparticle volume fraction. The dependencies of density ρ_w, dynamic viscosity μ_w, thermal conductivity κ_w, and specific heat capacity $c_{p,w}$ of water on temperature in the range 0–100 °C can be described by the polynomial interpolation of the experimental data [35]:

$$\begin{aligned}\rho_w &= 999.86 + 6.1238\cdot10^{-2}\,T - 8.3131\cdot10^{-3}\,T^2\\ &\quad + 6.4236\cdot10^{-5}\,T^3 - 3.9530\cdot10^{-7}\,T^4\\ &\quad + 1.0808\cdot10^{-9}\,T^5,\\ \mu_w &= 1.7825\cdot10^{-3} - 5.8439\cdot10^{-5}\,T + 1.2592\cdot10^{-6}\,T^2\\ &\quad - 1.6986\cdot10^{-8}\,T^3 + 1.2480\cdot10^{-10}\,T^4\\ &\quad - 3.7458\cdot10^{-13}\,T^5,\\ \kappa_w &= 0.5609 + 1.9488\cdot10^{-3}\,T - 1.0133\cdot10^{-6}\,T^2\\ &\quad - 1.2840\cdot10^{-7}\,T^3 + 6.2118\cdot10^{-10}\,T^4,\\ c_{p,w} &= 4218.79 - 3.1667\,T + 9.5040\cdot10^{-2}\,T^2\\ &\quad - 1.3890\cdot10^{-3}\,T^3 + 1.0722\cdot10^{-5}\,T^4\\ &\quad - 3.2042\cdot10^{-8}\,T^5,\end{aligned}$$

where T is the temperature in Celsius degrees. In what follows, we will also need the thermal expansion coefficient of water, which is defined by

$$\beta_T = -\frac{1}{\rho_w}\frac{\partial\rho_w}{\partial T}$$

and can be described by the polynomial

$$\begin{aligned}\beta_T &= -6.3516\cdot10^{-5} + 1.6839\cdot10^{-5}\,T - 1.9824\cdot10^{-7}\,T^2\\ &\quad + 1.6867\cdot10^{-9}\,T^3 - 5.7744\cdot10^{-12}\,T^4.\end{aligned}$$

The dependencies of density ρ_a, thermal conductivity κ_a, and specific heat capacity $c_{p,a}$ of alumina nanoparticles on temperature are given by [36]

$$\begin{aligned}&\rho_a = 3921.71 - 8.5625\cdot10^{-2}\,T, && 0\le T\le100\,^\circ\mathrm{C},\\ &\kappa_a = 5.5 + 34.5\exp(-0.0033\,T), && 0\le T\le1300\,^\circ\mathrm{C},\\ &c_{p,a} = 1044.60 + 0.1742(273.15+T) - \frac{2.796\cdot10^7}{(273.15+T)^2}, && T\le1500\,^\circ\mathrm{C}.\end{aligned}$$

Here the expression for density is based on the linear model

$$\rho = \rho_0(1-\beta_T(T-T_0)),$$

with the thermal expansion coefficient $\beta_T = 2.1843\cdot10^{-5}\,1/\mathrm{K}$ [37], $T_0 = 20\,^\circ\mathrm{C}$, $\rho_0 = 3920\,\mathrm{kg/m^3}$.

The density and specific heat capacity of nanofluid are determined according to

$$\begin{aligned}\rho &= C_v\rho_a + (1-C_v)\rho_w,\\ c_p &= \frac{C_v\rho_a c_{p,a} + (1-C_v)\rho_w c_{p,w}}{\rho},\end{aligned}\qquad(1)$$

where C_v is the volume fraction of nanoparticles. The viscosity and thermal conductivity of water-alumina nanofluid are given by the following correlations:

$$\begin{aligned}\mu &= \mu_w\exp\left(\frac{4.91C_v}{0.2092-C_v}\right),\\ \kappa &= \kappa_w(1+4.5503C_v).\end{aligned}$$

These correlations are valid in the range $20\le T\le80\,^\circ\mathrm{C}$, $0\le C_v\le0.06$ and based on the experimental data for alumina nanoparticles with the diameter of $d_a = 46\,\mathrm{nm}$ in water [13].

The diffusion coefficient is determined by the Einstein-Stokes formula [38]

$$\mathcal{D} = \frac{k_B T}{3\pi\mu_w d_a},$$

where d_a is the nanoparticle diameter and $k_B = 1.3807\times10^{-23}\,\mathrm{J/K}$ is the Boltzmann constant.

The dependence of nanofluid physical properties on temperature is shown in fig. 1 for different volume fractions of nanoparticles. When the volume fraction is increased, the density, viscosity, and thermal conductivity of nanofluid increase, while the specific heat capacity decreases. The diffusion coefficient does not depend on the nanoparticle volume fraction.

The thermophoretic velocity of nanoparticles is given by

$$\boldsymbol{v}_T = -\mathcal{D}_T\nabla T,\qquad(2)$$

where $\mathcal{D}_T$ is the thermophoretic mobility [31]. Then the nanoparticle flux (in $\mathrm{kg/m^2s}$) can be written as

$$\boldsymbol{\mathcal{J}} = -\rho(\mathcal{D}\nabla C_m + \mathcal{D}_T C_m\nabla T),\qquad(3)$$

where C_m is the mass fraction of nanoparticles, which is related to the volume fraction C_v by the formula

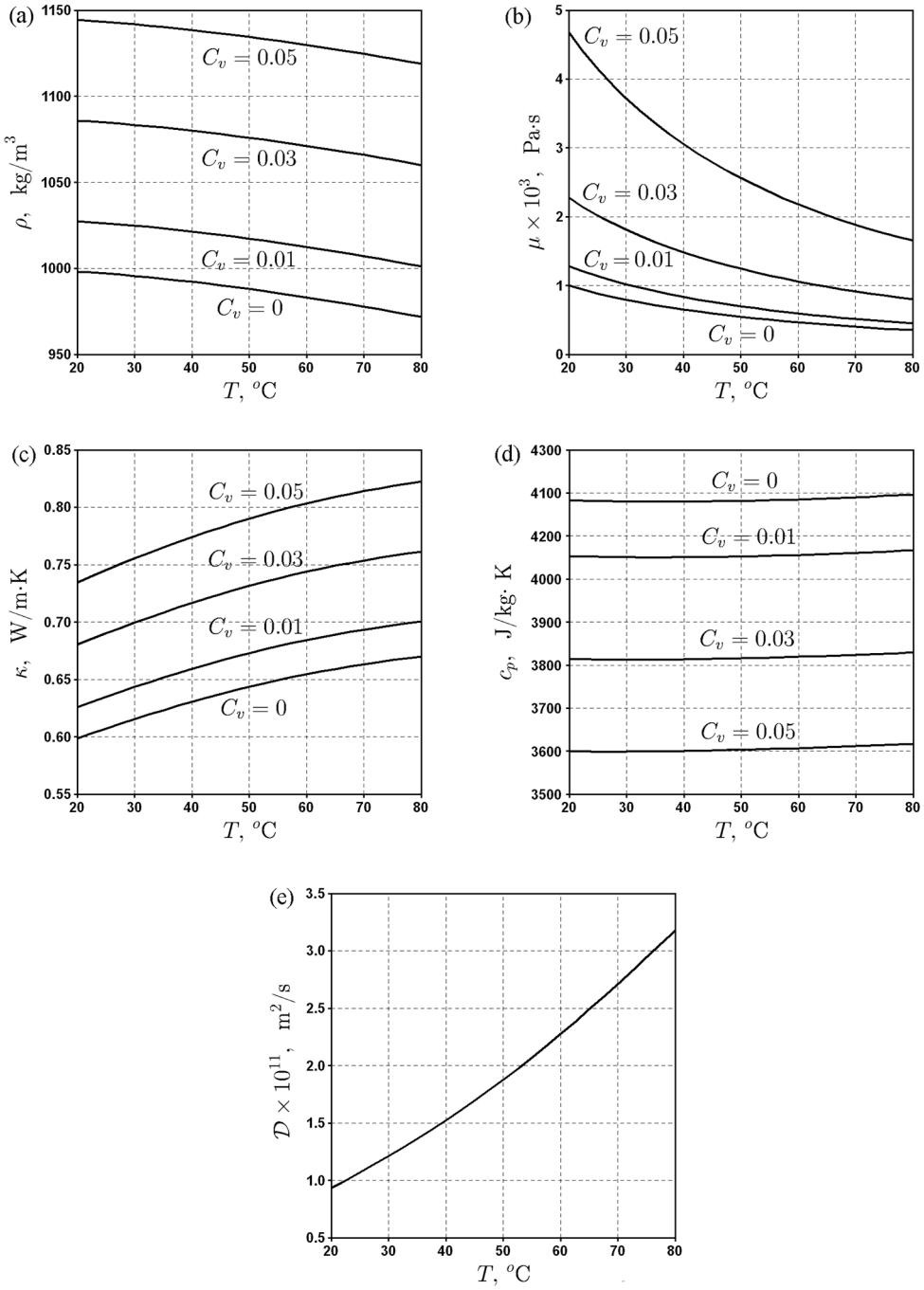

Fig. 1. Dependence of water-alumina nanofluid physical properties on temperature for different volume fractions of nanoparticles C_v: (a) density ρ; (b) dynamic viscosity μ; (c) thermal conductivity κ; (d) specific heat capacity c_p; (e) diffusion coefficient $\mathcal{D}$.

$\rho C_m = \rho_a C_v$. Here ρ is the nanofluid density (see eq. (1)) and ρ_a is the nanoparticle density. From the latter relation, one can obtain

$$C_m = \frac{\rho_a C_v}{C_v \rho_a + (1 - C_v)\rho_w},$$
$$C_v = \frac{\rho_w C_m}{C_m \rho_w + (1 - C_m)\rho_a}. \quad (4)$$

The Soret coefficient of nanofluid is defined by

$$\mathcal{S}_T = \mathcal{D}_T / \mathcal{D}. \quad (5)$$

For suspension of solid particles in liquid, the following formula for thermophoretic mobility was suggested in [30]:

$$\mathcal{D}_T = 0.26 \frac{\kappa_f}{2\kappa_f + \kappa_p} \frac{\mu_f}{\rho_f T}, \quad (6)$$

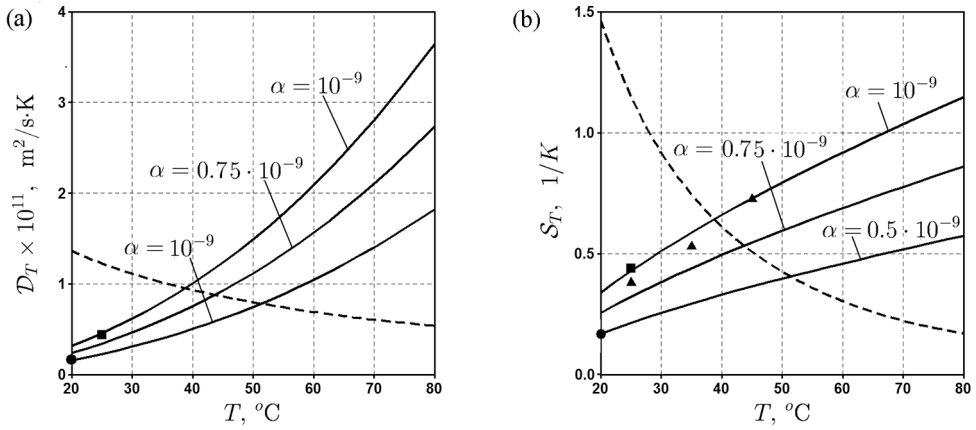

Fig. 2. The dependence of thermophoretic mobility $\mathcal{D}_T$ (a) and Soret coefficient $\mathcal{S}_T$ (b) on temperature for different values of parameter α. Solid lines correspond to formula (7), while the dashed line corresponds to formula (6) for $\mathcal{D}_T$. Experimental data: ● Fe_2O_3 ($d_p = 9.6$ nm) in cyclohexane [42], ■ Fe_3O_4 ($d_p = 10$ nm) in water [43], ▲ polystyrene ($d_p = 106$ nm) in water [40].

where the subscripts f and p correspond to fluid and particle, respectively. The above formula was obtained by matching the experimental data for micro-sized particles in water and n-hexane with theoretical expression derived for solid particles in gas [29], where the coefficient 3/4 was replaced by 0.26. The latter expression was in turn obtained by solving the problem of creeping flow past a solid sphere in a medium with a given temperature gradient. The conditions of impermeability as well as continuity of temperature and heat flux were imposed on the sphere surface. It was assumed that the tangential velocity component was proportional to the temperature gradient ("thermal creep" velocity condition).

Formula (6) was used for modelling thermophoresis in nanofluids in many works [1,8,23–27]. According to this expression, the thermophoretic mobility is proportional to the viscosity of the base fluid. Then the Soret coefficient (5) is proportional to the square of viscosity and quickly decreases with increasing temperature (the viscosity of liquids is typically a decreasing function of temperature), see fig. 2(b). However, this result contradicts numerous experimental data for colloidal suspensions [31, 32,39,40], where a significant increase of the Soret coefficient with temperature was observed. Theoretical studies [32] as well as molecular dynamics simulations [33] suggest that the thermophoretic mobility in colloidal suspensions is inversely proportional to the base fluid viscosity. In this case, the Soret coefficient does not depend on the viscosity. Note that this coefficient is the proportionality factor between temperature and concentration gradients in the stationary state and in the absence of convection (in this case, nanoparticle flux (3) vanishes, which leads to $\nabla C_m = -\mathcal{S}_T C_m \nabla T$). Thus, the independence of Soret coefficient from the hydrodynamic quantities (viscosity) seems to be quite reasonable [39].

The mechanisms, which induce nanoparticle drift in colloidal suspensions under the action of temperature gradient, are rather complicated and depend on the properties of solvent, nanoparticles, and additives, which prevent particle agglomeration and ensure the stability of colloid. According to [32], the main mechanisms are thermoosmosis in the electric double layer, thermoelectric effect, dispersion forces, thermal diffusion. In real nanofluids, the thermophoretic motion results from the net action of all these mechanisms. Thus, it is not possible to provide a general formula for $\mathcal{D}_T$, which can be applicable to all nanofluids. For concrete systems, this coefficient can be determined experimentally. At the same time, a through analysis of the available experimental data and theoretical concepts for a wide range of colloidal systems allows one to ascertain some general properties of $\mathcal{D}_T$. This coefficient

1) Does not depend on the particle size [40].
2) Is inversely proportional to the solvent viscosity μ_f [32, 33].
3) Is directly proportional to the thermal expansion coefficient of the solvent β_T [39].
4) Is directly proportional to the expression $3\kappa_f(2\kappa_f + \kappa_p)^{-1}$ [32,41].

The latter expression is related to the change of temperature gradient near the particle surface due to the difference between thermal conductivities of the particle κ_p and the solvent κ_f.

On the basis of these results, we suggest the following expression for thermophoretic mobility:

$$\mathcal{D}_T = \alpha \frac{\beta_T}{\mu_f} \frac{\kappa_f}{2\kappa_f + \kappa_p}, \tag{7}$$

where α is the proportionality coefficient, which is chosen in such a way that the order of $\mathcal{D}_T$ must correspond to the experimental data. Formula (7) should be viewed as an empirical model, which predicts the behaviour of $\mathcal{D}_T$ in accordance with the existing experimental data and theoretical concepts.

The dependence of thermophoretic mobility and the Soret coefficient on temperature is shown in fig. 2. These coefficients were determined on the basis of formula (7) as well as formula (6). The curves, which correspond to

formula (7), correctly predict the increase of Soret coefficient with temperature. The order of $\mathcal{S}_T$ is in agreement with the experimental data for water-based colloids [39, 40] as well as organic and aqueous solutions of iron oxide nanoparticles [42,43]. At the same time, the Soret coefficient $\mathcal{S}_T$ determined on the basis of formula (6) for $\mathcal{D}_T$ decreases with temperature. It contradicts the experimental data.

Unfortunately, there is no experimental data for thermophoretic mobility of water-alumina nanofluid in the literature. In the calculations below, we use formula (7) with $\alpha = 10^{-9}$, $\mu_f = \mu_w$, $\kappa_f = \kappa_w$, $\kappa_p = \kappa_a$. To understand how the intensity of thermophoresis affects heat and mass transfer, calculations are also performed for $\alpha = 0.5 \cdot 10^{-9}$ and $\alpha = 0.75 \cdot 10^{-9}$.

3 Forced convection in a circular tube: problem statement

Let us consider forced convection of water-alumina nanofluid in a circular tube of radius R (fig. 3). The flow is assumed to be laminar and axisymmetric. Nanofluid enters the tube at $z = 0$ with temperature T_0 and volume fraction of nanoparticles C_{v0}. The velocity profile at the entrance is parabolic

$$v(r) = 2v_0 \left(1 - \left(\frac{r}{R}\right)^2\right), \tag{8}$$

where v_0 is the average velocity. A constant heat flux q is imposed on the wall $0 \le z \le L$. The following values of parameters are used in the calculations: $R = 0.001\,\mathrm{m}$, $L = 1\,\mathrm{m}$.

The nanofluid is described by a generalization of a two-component model suggested in [8] to compressible flows with variable physical properties. The compressibility effect is associated with the dependence of density on temperature and nanoparticle volume fraction according to (1). For computations, it is convenient to use mass fraction C_m, which is related to the volume fraction C_v by the first formula in (4). The equations of momentum, continuity, energy, and nanoparticle transfer are written as

$$\partial_t(\rho \boldsymbol{u}) + \nabla \cdot (\rho \boldsymbol{u}\boldsymbol{u}) = -\nabla p + \nabla \cdot \Pi, \tag{9}$$

$$\partial_t \rho + \nabla \cdot (\rho \boldsymbol{u}) = 0, \tag{10}$$

$$\partial_t(\rho H) + \nabla \cdot (\rho \boldsymbol{u} H) = \nabla \cdot (\kappa \nabla T), \tag{11}$$

$$\partial_t(\rho C_m) + \nabla \cdot (\rho \boldsymbol{u} C_m) = \nabla \cdot (\rho \mathcal{D} \nabla C_m + \rho \mathcal{D}_T C_m \nabla T), \tag{12}$$

$$\Pi = \mu \left(\nabla \boldsymbol{u} + \nabla \boldsymbol{u}^T - \frac{2}{3} \nabla \cdot \boldsymbol{u} E\right), \quad H = \int_{T_0}^{T} c_p \mathrm{d}T.$$

Here Π is the viscous stress tensor, E is the unit tensor, $\boldsymbol{u}\boldsymbol{u}$, $\nabla \boldsymbol{u}$ are the dyadic products, and H is the specific enthalpy. Since the dependence of specific heat capacity on temperature is very weak (see fig. 1(d)), we assume that c_p corresponds to the inlet temperature T_0. In this case, the enthalpy is determined by the formula

Fig. 3. Geometry of the tube and computational grid ($R = 0.001$ m, $L = 1$ m). The arrows show the directions of clustering. The number above the arrow (or on the right) is the number of cells, while the number below the arrow (or on the left) is the ratio of neighboring cell sizes.

$$H = c_p(T_0, C_v)(T - T_0). \tag{13}$$

In what follows, we consider the stationary equations (9)–(12) in cylindrical coordinates (r, z) taking into account the axial symmetry. The velocity vector has the form $\boldsymbol{u} = (u, v)$, where u is the radial velocity and v is the axial velocity. The governing equations are rewritten in cylindrical coordinates.

The boundary conditions have the form

$$r = 0: \qquad \frac{\partial u}{\partial r} = \frac{\partial v}{\partial r} = \frac{\partial T}{\partial r} = \frac{\partial C_m}{\partial r} = 0, \tag{14}$$

$$r = R: \qquad u = v = 0, \qquad \kappa \frac{\partial T}{\partial r} = q, \quad 0 \le z \le L,$$

$$\mathcal{D} \frac{\partial C_m}{\partial r} + \mathcal{D}_T C_m \frac{\partial T}{\partial r} = 0, \tag{15}$$

$$z = 0: \qquad u = 0, \qquad v = v(r), \qquad T = T_0,$$

$$C_m = C_{m0}, \tag{16}$$

$$z = L: \qquad \frac{\partial u}{\partial z} = \frac{\partial v}{\partial z} = \frac{\partial T}{\partial z} = \frac{\partial C_m}{\partial z} = 0. \tag{17}$$

The velocity profile $v(r)$ is given by (8). The value of mass fraction C_{m0} at the inlet is determined from a given volume fraction C_{v0} with the help of the first formula in (4). Conditions (14) impose the axial symmetry of the problem, while conditions (17) correspond to a fully developed flow at the outlet.

In addition to the two-component model of nanofluid with thermophoresis, the one-component model will be also used for calculations. In the latter model, the physical properties of nanofluid correspond to the constant volume fraction of nanoparticles at the inlet, while the nanoparticle transfer equation (12) and the corresponding boundary conditions are omitted. The comparison between the two models will be performed in sect. 4.

The governing equations are solved numerically with the help of ANSYS Fluent 14.5. The characteristics of computational grid are shown in fig. 3. The clustering in the direction of tube wall $r = R$ is introduced in order to correctly resolve the thermal and concentration boundary layers. The grid also has clustering in the directions

of inlet $z = 0$ and outlet $z = L$. The choice of grid parameters was made by comparing the numerical solution with the analytical one [28] for the case of constant physical properties (see below). The problem is solved iteratively by the SIMPLEC algorithm (Semi-Implicit Method for Pressure-Linked Equations – Consistent). The second-order approximation is used. The variable physical properties and aspect ratio of the tube ($L/R = 1000$) resulted in a large number of iterations required to achieve convergence (around 6000).

The transport of heat in the tube is characterized by *the heat transfer coefficient*, which is defined by

$$h = \frac{q}{T(R,z) - T_b(z)}, \tag{18}$$

where q is the wall heat flux, $T(R,z)$ is the wall temperature, and $T_b(z)$ is the bulk temperature in the tube. The average heat transfer coefficient is calculated by averaging h over the heated section of the tube

$$\overline{h} = \frac{1}{2\pi RL}\int_0^L \int_0^{2\pi} hR\mathrm{d}\varphi\mathrm{d}z.$$

The bulk temperature $T_b(z)$ can be determined from the bulk specific enthalpy H_b

$$H_b = \frac{\int_0^{2\pi}\int_0^R H\rho v r\mathrm{d}r\mathrm{d}\varphi}{\int_0^{2\pi}\int_0^R \rho v r\mathrm{d}r\mathrm{d}\varphi},$$

$$H_b = c_p(T_0, C_{vb})(T_b - T_0), \tag{19}$$

where H is given by (13), and C_{vb} is the bulk concentration defined as

$$C_{vb} = \frac{\int_0^{2\pi}\int_0^R C_v v r\mathrm{d}r\mathrm{d}\varphi}{\int_0^{2\pi}\int_0^R v r\mathrm{d}r\mathrm{d}\varphi}.$$

The bulk temperature can be estimated by a simple formula, which is valid for the case of constant physical properties [44]

$$T_b(z) = T_0 + \frac{2q}{Rv_0\rho c_p}z, \tag{20}$$

where the density ρ and specific heat capacity c_p correspond to the inlet temperature.

The main dimensionless parameters, which characterize the similarity of hydrodynamic, thermal, and diffusion regimes in the tube, are the Reynolds number, thermal Peclet number, and solutal Peclet number, respectively:

$$\mathrm{Re} = \frac{\rho v_0 2R}{\mu}, \qquad \mathrm{Pe} = \frac{\rho c_p v_0 2R}{\kappa}, \qquad \mathrm{Pe}_c = \frac{v_0 2R}{\mathcal{D}}.$$

The dimensionless parameters that characterize heat transport in the tube are the local and average Nusselt numbers:

$$\mathrm{Nu} = \frac{h2R}{\kappa},$$

$$\overline{\mathrm{Nu}} = \frac{1}{2\pi RL}\int_0^L \int_0^{2\pi} \mathrm{Nu}R\mathrm{d}\varphi\mathrm{d}z. \tag{21}$$

Table 1. The list of calculated cases for the heating regime ($q = 10000\,\mathrm{W/m^2}$). The values of v_0 (m/s), Re and Pe correspond to the tube inlet.

	$C_{v0} = 0$		$C_{v0} = 0.01$		$C_{v0} = 0.03$	
Pe	Re	v_0	Re	v_0	Re	v_0
1000					78	0.1437
1250	179	0.0896	151	0.0939	98	0.0821
1500	215	0.1075	181	0.1127	118	0.1027
1750	250	0.1254	211	0.1315	137	0.1438
2000	286	0.1434	241	0.1503	157	0.1643
2500	358	0.1792	302	0.1879	196	0.2054
3000	429	0.2150	362	0.2254	235	0.2464
4000	572	0.2867	482	0.3006	313	0.3286
5000	715	0.3584	603	0.3757	392	0.4107
6000	858	0.4301	724	0.4509	470	0.4929
7000	1001	0.5018	844	0.5260	549	0.5750
8000	1144	0.5734	965	0.6012	627	0.6572
9000	1287	0.6451	1086	0.6763	705	0.7393

Table 2. The list of calculated cases for the cooling regime ($q = -10000\,\mathrm{W/m^2}$). The values of v_0 (m/s), Re and Pe correspond to the tube inlet.

	$C_{v0} = 0$		$C_{v0} = 0.01$		$C_{v0} = 0.03$	
Pe	Re	v_0	Re	v_0	Re	v_0
800					198	0.0751
1000	451	0.0822	381	0.0860	247	0.0938
1250	564	0.1027	476	0.1076	309	0.1173
1500	677	0.1233	571	0.1291	371	0.1407
1750	790	0.1438	666	0.1506	432	0.1642
2000	903	0.1643	761	0.1721	494	0.1876
2500	1128	0.2054	951	0.2151	618	0.2346
3000	1354	0.2465	1142	0.2581	741	0.2815
4000	1805	0.3287	1522	0.3442	988	0.3753
5000	2256	0.4109	1903	0.4302	1236	0.4691
6000			2283	0.5163	1483	0.5629
7000					1730	0.6567
8000					1977	0.7506
9000					2224	0.8444

In this paper, we investigate the flow and heat transfer of a nanofluid in a tube under heating and cooling conditions. The lists of calculated cases are presented in tables 1 and 2. The values of Peclet and Reynolds numbers as well

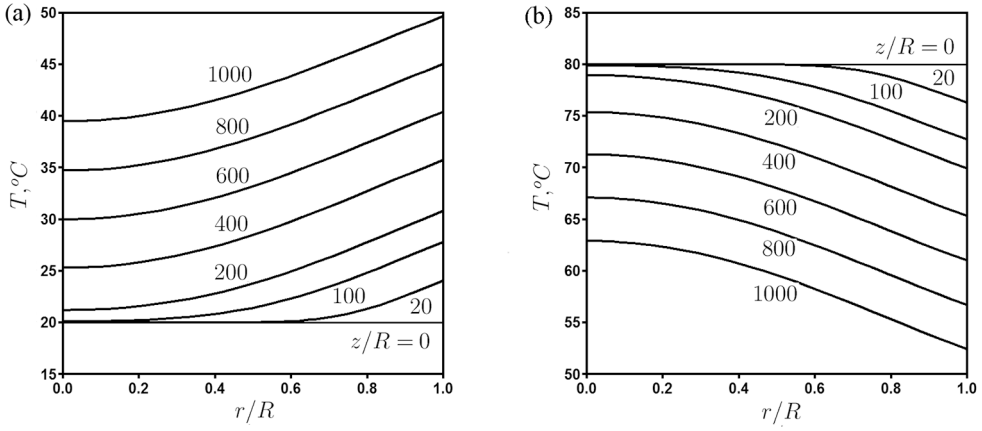

Fig. 4. Temperature field in the sections of constant axial coordinate for Pe = 2500, $C_{v0} = 0.03$: (a) heating regime, (b) cooling regime.

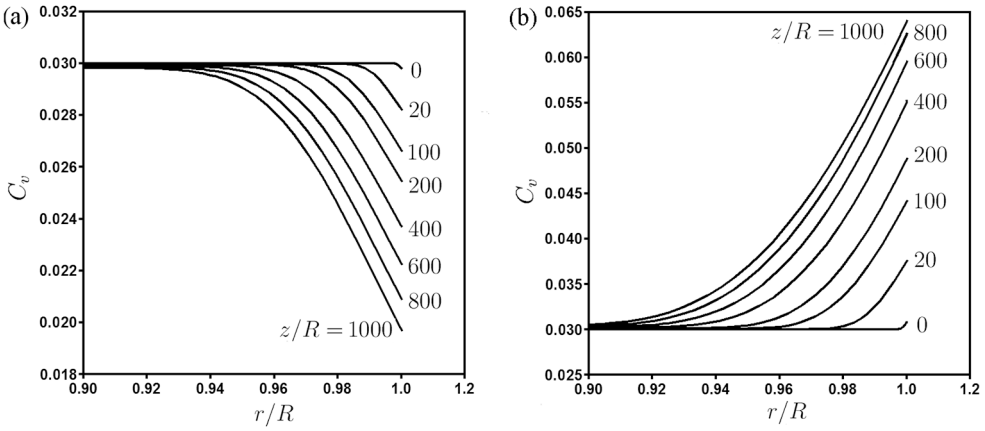

Fig. 5. Nanoparticle volume fraction in the sections of constant axial coordinate for Pe = 2500, $C_{v0} = 0.03$: (a) heating regime, (b) cooling regime.

as inlet velocity are given for different nanoparticle volume fractions. The thermal conditions are as follows. The inlet temperature and the heat flux are $T_0 = 20\,^\circ\mathrm{C}$ and $q = 10000\,\mathrm{W/m^2}$ for the heating regime, while $T_0 = 80\,^\circ\mathrm{C}$ and $q = -10000\,\mathrm{W/m^2}$ for the cooling regime. The heat transfer performance can be characterized by the dependencies of heat transfer coefficient and Nusselt number on the thermal Peclet number for different volume fractions of nanoparticles. The Peclet number is proportional to the average inlet velocity v_0. Note that this velocity cannot be too small since in this case the outlet temperature may exceed the boiling temperature of nanofluid under heating or descend below the freezing point under cooling (in case of water, these temperatures are $100\,^\circ\mathrm{C}$ and $0\,^\circ\mathrm{C}$, respectively, at normal pressure). At the same time, this velocity cannot be too large since laminar axisymmetric flow is replaced by the turbulent flow at $\mathrm{Re} \approx 2300$.

One can also take into account that the dependence of physical properties on temperature leads to a significant change of the Reynolds and Peclet numbers along the tube at the same average inlet velocity v_0. In particular, the decrease of viscosity with temperature (see fig. 1(b)) results in the downstream increase of the Reynolds number when the tube is heated with a constant heat flux. In what follows, we assume the values of Re and Pe correspond to the temperature and nanoparticle volume fraction at the inlet. From the presented considerations it is clear that the laminar flow of nanofluid in the tube can be realized in some range of Peclet (Reynolds) numbers.

4 Results and discussion

In this paper, we analyze the numerical results on the basis of full non-linear model (9)-(17). Along with the results for two-component model also the comparative results for one-component model are presented. Let us first investigate the flow and heat transfer of a nanofluid in a tube when $C_{0v} = 0.03$ and $\mathrm{Pe} = 2500$.

Temperature profiles in the cross-sections of the tube, which correspond to constant values of axial coordinate, are shown in fig. 4. Temperature is gradually rising along the tube in the heating regime and is falling in the cooling regime. The temperature gradients in the heated sec-

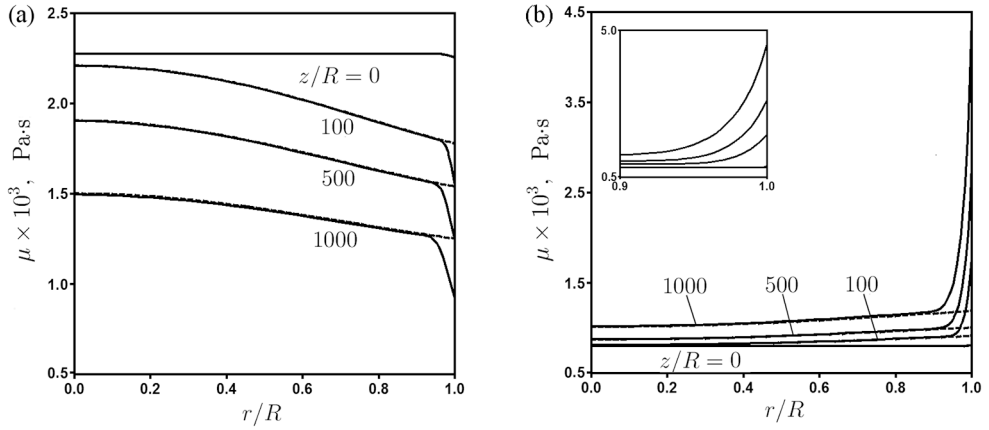

Fig. 6. Viscosity in the sections of constant axial coordinate for Pe = 2500, $C_{v0} = 0.03$. Results for one-component (dashed curves) and two-component (solid curves) models: (a) heating regime, (b) cooling regime.

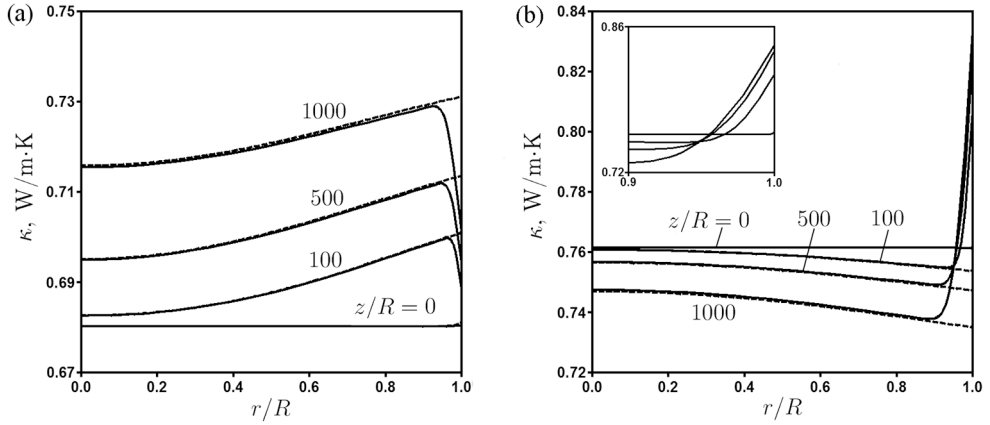

Fig. 7. Thermal conductivity in the sections of constant axial coordinate for Pe = 2500, $C_{v0} = 0.03$. Results for one-component (dashed curves) and two-component (solid curves) models: (a) heating regime, (b) cooling regime.

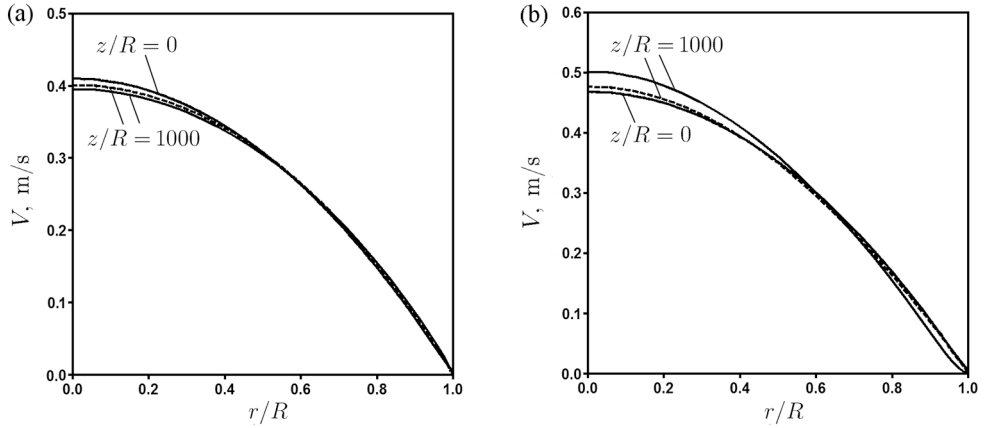

Fig. 8. Velocity profiles in the sections of constant axial coordinate for Pe = 2500, $C_{v0} = 0.03$. Results for one-component (dashed curves) and two-component (solid curves) models: (a) heating regime, (b) cooling regime.

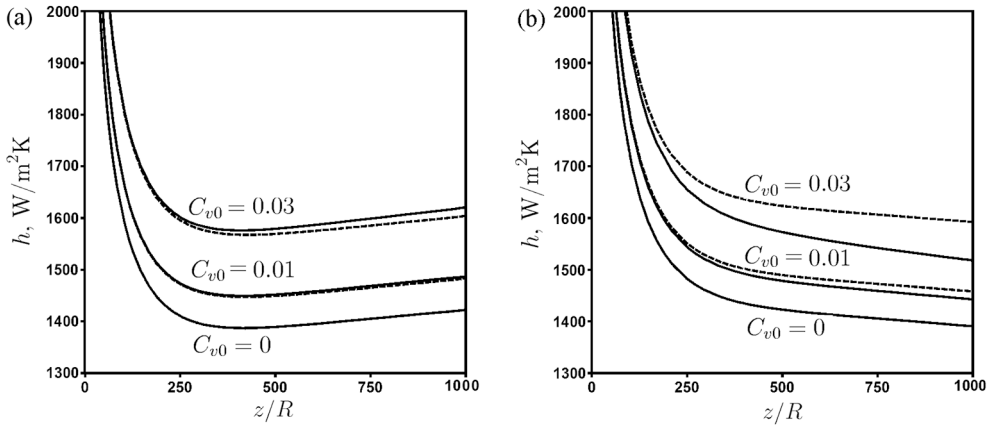

Fig. 9. Local heat transfer coefficient for Pe = 2500. Results for one-component (dashed curves) and two-component (solid curves) models: (a) heating regime, (b) cooling regime.

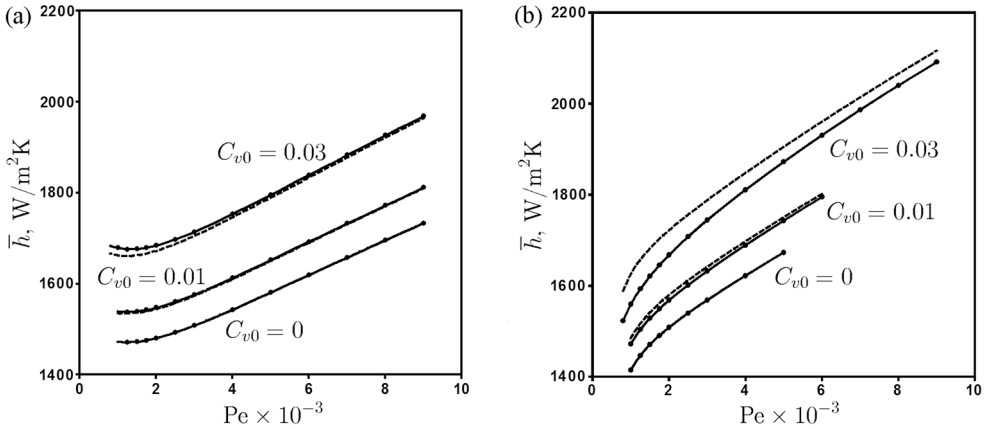

Fig. 10. Average heat transfer coefficient. Results for one-component (dashed curves) and two-component (solid curves) models: (a) heating regime, (b) cooling regime.

tion induce nanoparticle volume fraction gradients due to thermophoresis, see fig. 5. Nanoparticles are driven in the direction of lower temperature, *i.e.* from the wall to the center of the tube under heating and from the center of the tube to the wall under cooling. Note that the variation of nanoparticle concentration under cooling is greater than that under heating. It happens because the increase of concentration itself intensifies thermophoresis, which, in its turn, causes further separation of nanofluid, see (3).

When the Peclet number is large, noticeable variations of nanoparticle volume fraction occur only in a thin boundary layer near the tube wall. The largest thermophoretic separation is achieved at the end of the heated section near the tube wall, where nanoparticle volume fraction decreases by 33% under heating and increases by more than twice under cooling with respect to the inlet value $C_{v0} = 0.03$. Note that the condition of zero axial derivative of C_m (see (17)) does not affect the nanoparticle volume fraction profile inside the tube due to strong convective flow in the axial direction.

The variations of nanoparticle volume fraction in the radial direction result in the variations of viscosity and thermal conductivity (figs. 6 and 7). One can see the decrease of viscosity and thermal conductivity near the tube wall under heating and the increase of these properties under cooling.

The nanoparticle migration caused by the temperature gradient is not taken into account in the one-component model. It explains the difference in numerical results between the two models. The velocity profile in the model with thermophoresis is modified slightly stronger than that in the model without thermophoresis (fig. 8), where only the temperature dependence of the physical properties is considered. The viscosity reduction (growth) in the two-component model leads to the increase (decrease) of velocity near the wall under heating (cooling). At the tube center, the velocity profile, conversely, is flattened (elongated) in order to keep the mass flow rate constant.

To show the influence of thermophoretic effect on heat transfer, the local heat transfer coefficient h was calculated from (18). The corresponding curves are shown in fig. 9 for different C_{v0} at the inlet. As one can see, after a significant drop at the entrance region, a gradual increase of the local heat transfer coefficient is observed under heating and a

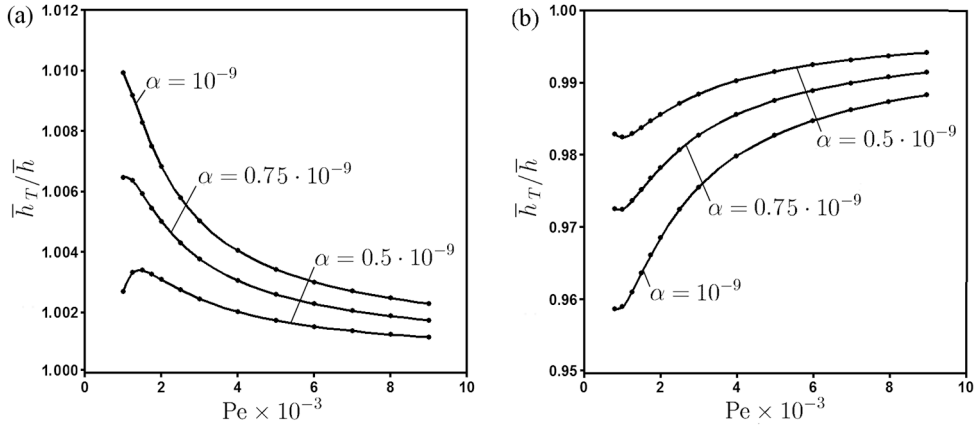

Fig. 11. Relative average heat transfer coefficient for $C_{v0} = 0.03$, $\alpha = 0.5 \cdot 10^{-9}$, $\alpha = 0.75 \cdot 10^{-9}$, $\alpha = 1 \cdot 10^{-9}$: (a) heating regime, (b) cooling regime.

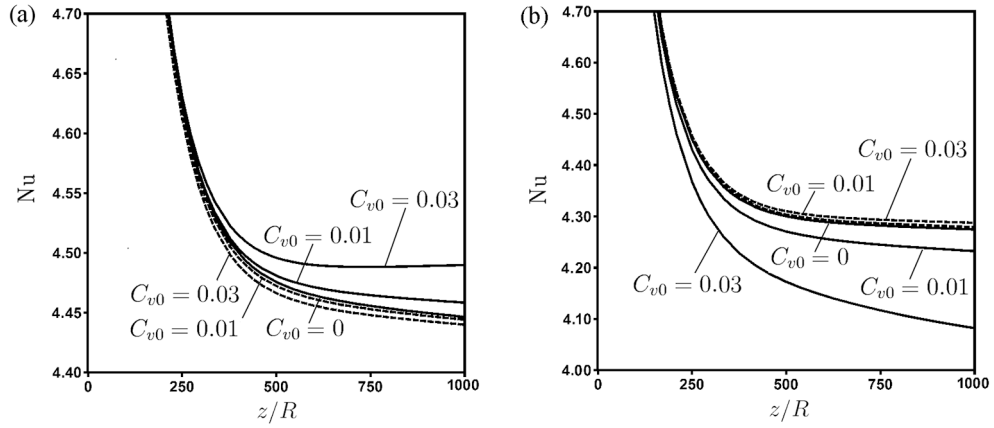

Fig. 12. Local Nusselt number for Pe = 2500. Results for one-component (dashed curves) and two-component (solid curves) models: (a) heating regime, (b) cooling regime.

slight decrease further downstream under cooling. The increase of nanoparticle volume fraction leads to the increase of h in both thermal regimes. The calculations on the basis of the two-component model provide larger values of h in comparison with the one-component model in the heating regime, see fig. 9(a), but under cooling the effect is opposite and stronger, see fig. 9(b). The differences of h between two thermal regimes and between two models can be explained by the velocity increase (decrease) near the wall due to viscosity reduction (growth) in the boundary layer. The latter tendency is caused by thermophoresis.

The dependence of the average heat transfer coefficient $\overline{h}$ on Pe for different C_{v0} at the inlet is presented in fig. 10. The dots correspond to the cases listed in tables 1 and 2. The coefficient $\overline{h}$ increases with C_{v0} and Pe, and the curves have different forms for different thermal regimes. The values of $\overline{h}$ corresponding to the one- and two-component models deviate for higher values of C_{v0}. It is worth noting that in the cooling regime the deviation is greater than that under heating, wherein this effect is noticeable only at low Pe and high C_{v0}. Actually, the coefficient $\overline{h}$ reflects the same tendencies as h. Thus, as it was observed for h under heating, the coefficient $\overline{h}$ for the model with thermophoresis is higher compared to the model without thermophoresis, and for low Pe the difference is about 1% for $C_{v0} = 0.03$. When cooling, the deviation between values of $\overline{h}$ for two models is the opposite and hardly exceeds 4% for high C_{v0}.

The influence of thermophoretic intensity on heat transfer is shown by fig. 11. This figure presents the ratio of average heat transfer coefficients in the two- ($\overline{h}_T$) and one-component ($\overline{h}$) models depending on Pe for different values of the coefficient α, which characterizes the intensity of thermophoresis (see (7)). As one can see, the intensification of thermophoresis enlarges the difference between $\overline{h}_T$ and $\overline{h}$ for both thermal regimes. Furthermore, the ratios $\overline{h}_T/\overline{h} > 1$ (fig. 11(a)) and $\overline{h}_T/\overline{h} < 1$ (fig. 11(b)) convince us that the increase and decrease of heat transfer coefficient due to thermophoretic effect under heating and cooling, respectively, reflect the corresponding rise and reduction of heat transfer intensity along the tube.

The local Nusselt number is shown in fig. 12 for Pe = 2500. It was calculated according to (21), where the thermal conductivity was determined at the bulk temperature

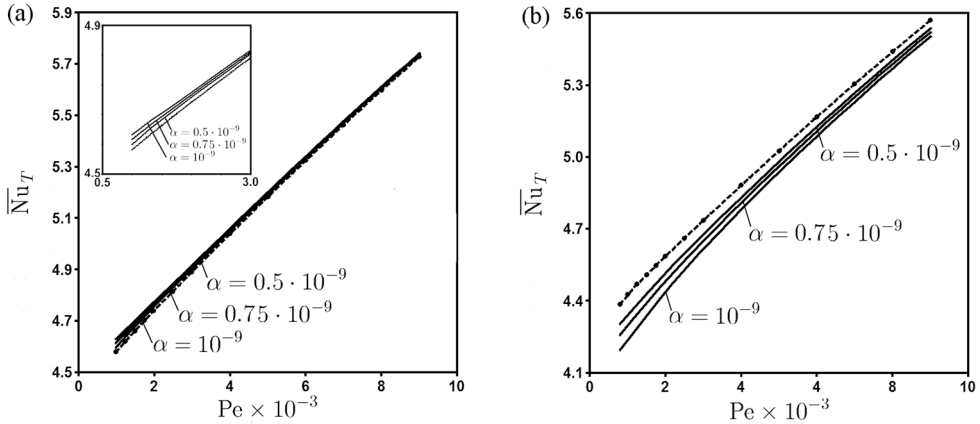

Fig. 13. Average Nusselt number for $C_{v0} = 0.03$, $\alpha = 0.5 \cdot 10^{-9}$, $\alpha = 0.75 \cdot 10^{-9}$, $\alpha = 1 \cdot 10^{-9}$: (a) heating regime, (b) cooling regime.

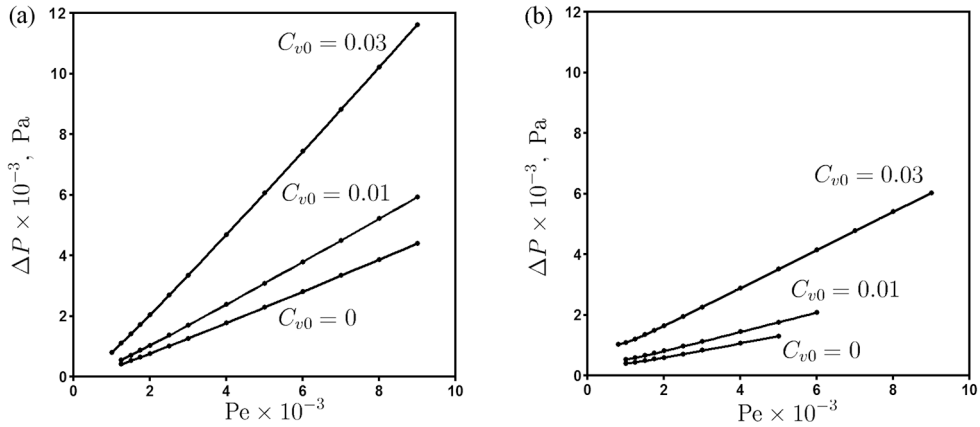

Fig. 14. Pressure drop on the basis of two-component model: (a) heating regime, (b) cooling regime.

$T_b(z)$. The calculations for the two-component model also predict the increase of Nu with increasing C_{v0} under heating. The Nusselt number characterizes the relative importance of convective and conductive heat transfer. When cooling, the reduction of Nu can be observed in fig. 12(b). It means the weakening of heat transfer by convection with the raise of C_{v0} due to thermophoresis. When heating, according to fig. 12(a), the heat transfer is, conversely, more intensive. It happens because convection along the tube in the wall region is more significant.

The dependence of the average Nusselt number on the thermal Peclet number calculated for $C_{v0} = 0.03$ at different values of α is presented in fig. 13. When heating (cooling), Nu is lower (higher) for the one-component model than for the two-component model in the whole range of Pe and its values rise (fall) with the growth of α. All these tendencies confirm the fact that thermophoresis slightly enhances heat transfer along the tube in the heating regime and affects conversely in the cooling regime.

The dependence of pressure drop in the heated section on the thermal Peclet number is shown in fig. 14. The calculations are based on the two-component model. The increase of nanoparticle volume fraction results in the significant rise of the required pressure drop at fixed Pe in both thermal regimes, and these tendencies in both cases are similar. Ratios of pressure drops calculated on the basis of two- (ΔP_T) and one-component (ΔP) models are presented in fig. 15 for $C_{v0} = 0.03$. There depicted variations of pressure drop with the increase of α. The results show opposite tendencies for heating and cooling. Noting that the ratio $\Delta P_T/\Delta P < 1$ under heating ($\Delta P_T/\Delta P > 1$ under cooling), we can say that the intensification of thermophoresis slightly reduces (raises) ΔP_T relatively to ΔP under heating (cooling). It happens due to viscosity decrease (increase) caused by reduction (growth) of nanoparticle volume fraction near the wall depending on the thermal regimes. The reduction (rise) of pressure drop depending on α for heating (cooling) is up to 2.5–4% (6–13%) for low Pe. With the growth of Pe, the curves approach unity more closely.

The dependence of wall shear stress

$$\tau_w = \mu \frac{\partial v}{\partial r}\bigg|_{r=R}$$

on the dimensionless axial coordinate z/R is presented in fig. 16. The wall shear stress decreases (increases) along

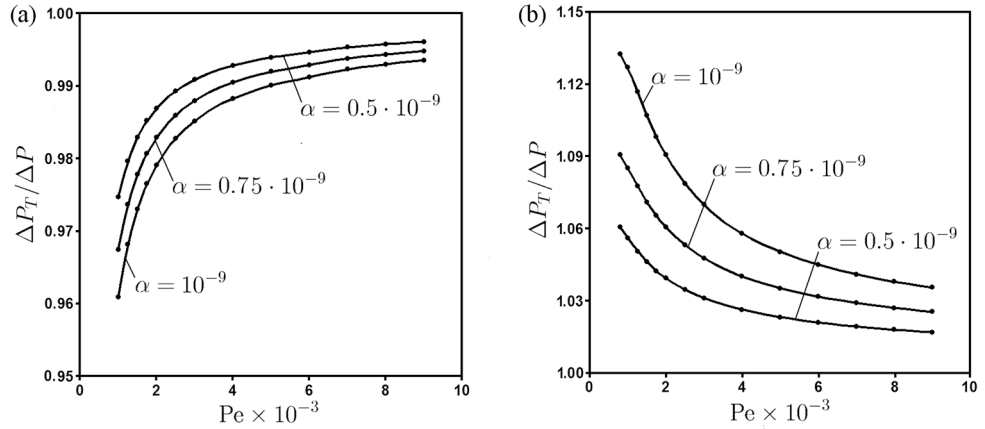

Fig. 15. Relative pressure drop for $C_{v0} = 0.03$, $\alpha = 0.5 \cdot 10^{-9}$, $\alpha = 0.75 \cdot 10^{-9}$, $\alpha = 1 \cdot 10^{-9}$: (a) heating regime, (b) cooling regime.

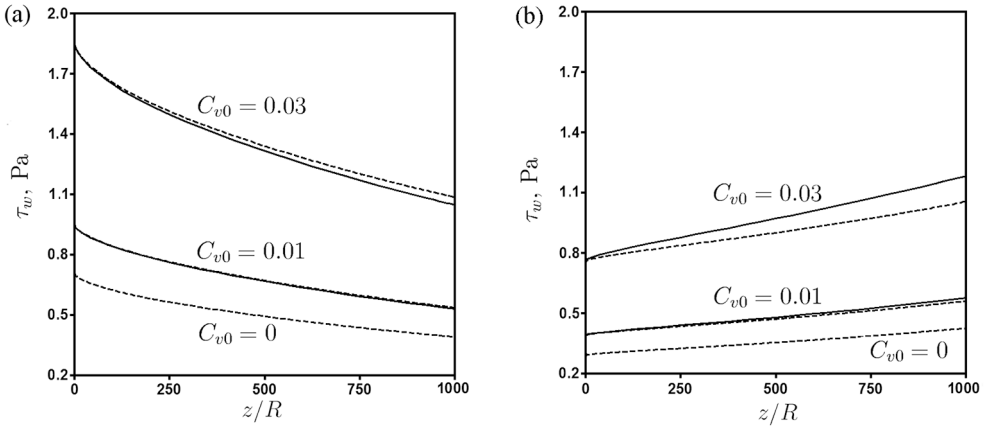

Fig. 16. Wall shear stress for Pe = 2500. Results for one-component (dashed curves) and two-component (solid curves) models: (a) heating regime, (b) cooling regime.

the channel under heating (cooling) due to the temperature dependence of viscosity. In the heating regime, τ_w is always lower for the model with thermophoresis than for the model without thermophoresis. When cooling, the deviations of τ_w for the two models are opposite and greater. It can be explained by variations of C_{v0} and, consequently, viscosity μ near the wall due to thermophoretic effect. As nanoparticle concentration increases near the wall more significantly under cooling than it decreases under heating, so does μ. We also note that the growth of C_{v0} leads to the additional increase of the wall shear stress in both thermal regimes.

The illustration of effectiveness of water-alumina nanofluid with different nanoparticle volume fractions in comparison with the base fluid is presented in fig. 17. The average heat transfer coefficient is plotted against the pumping power in the heated section, which is calculated according to $W_p = \Delta PQ$, where $Q = v_0\pi R^2$ is the volume flow rate. The increase of $\overline{h}$ with the growth of W_p takes place in both thermal regimes. Thus, as one can see in fig. 17, the growth of alumina nanoparticles concentration can improve the effectiveness of heat transfer in the whole range of pumping power calculated in this work. When heating, the improvement of heat transfer at low W_p is quite noticeable. At $C_{v0} = 0.3$ the average heat transfer coefficient is up to 12% higher compared to the base fluid. At high W_p the improvement of $\overline{h}$ is about 6.5%. In the cooling regime the enhancement of $\overline{h}$ with increasing C_{v0} hardly attains 3.5% even for low W_p. The difference in improvements of $\overline{h}$ with the growth of C_{v0} between two regimes can be explained by the pressure drop variations (see fig. 15) due to thermophoresis. At any fixed W_p the pressure drop rises with the growth of C_{v0} because of viscosity increase. However, thermophoresis decreases (increases) the pressure drop in the heating (cooling) regime. It means that, to keep the pumping power constant, v_0 must be raised (reduced). Thus, the increase of v_0 under heating noticeably enhances $\overline{h}$ with the growth of C_{v0}, but the correspondent decrease of v_0 under cooling makes $\overline{h}$ rise much less. Figure 17

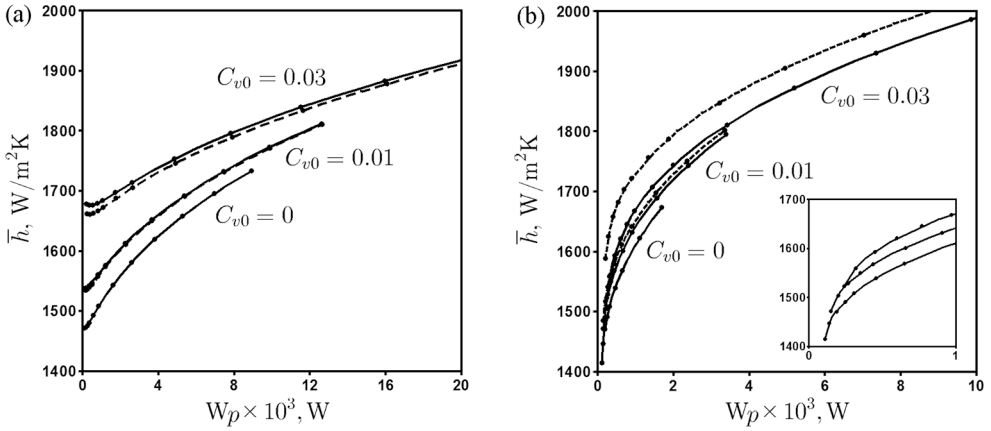

Fig. 17. The dependence of average heat transfer coefficient on pumping power at Pe = 2500. Results for one-component (dashed curves) and two-component (solid curves) models: (a) heating regime, (b) cooling regime.

shows that when heating (cooling), the curves of $\overline{h}$ for the two-component model are higher (lower) than for the one-component model, because in the latter case variations of the pressure drop due to thermophoresis are not taken into account.

Let us finally compare the effectiveness of water–alumina nanofluid applied to cooling and heating regimes. The analysis of the average heat transfer coefficient depending on pumping power shows the specific performance of considered nanofluid in each thermal regime. However, $\overline{h}$ calculated on the basis of two-component model is higher (lower) *versus* that for the one-component model under heating (cooling) for all Pe. The difference grows with increasing C_{v0}. Thus, we can say that thermophoretic effect near the tube wall slightly raises the effectiveness of heat transfer downstream under heating and slightly reduces it under cooling. Besides, the reduction is a little greater than the rise. We may finally conclude that the water-alumina nanofluid is less effective in the cooling regime in comparison to the heating regime due to thermophoretic effect.

5 Conclusion

In this paper, we have investigated the laminar convective heat transfer of water–alumina nanofluid in a circular tube with uniform heat flux. The investigation was performed for the heating and cooling regimes allowing for variable physical properties of nanofluid and a comparative analysis was made. The physical properties of the base fluid and the nanofluid are taken from experimental measurements. The nanofluid is described by a generalization of non-homogeneous two-component model to the case of compressible flow when the density depends on temperature and nanoparticle volume fraction. This model takes into account nanoparticle transport by convection, Brownian diffusion, and thermophoresis. The intensity of thermophoresis is characterized by the new empirical model for thermophoretic mobility. Homogeneous one-component model is also used in this study. It has been found that thermophoresis leads to a significant reduction (growth) of nanoparticle volume fraction in a thin boundary layer near the wall in the heating (cooling) regime. As a consequence, the decrease (increase) of viscosity and thermal conductivity in the wall region is observed. The viscosity reduction (growth) leads to the increase (decrease) of velocity near the wall under heating (cooling), while near the tube axis the velocity profile is flattened (elongated) in order to keep the mass flow rate constant. Thermophoretic migration of nanoparticles causes the reduction of wall shear stress, and, correspondingly, the required pressure drop in the heated section under heating and the increase of these properties under cooling.

The calculations on the basis of the two-component model provide higher (lower) values of the local and average heat transfer coefficients in comparison with the one-component model under heating (cooling). The results for the two-component model predict the increase of Nusselt number with increasing nanoparticle volume fraction and the intensity of thermophoresis in the heating regime and the corresponding decrease of Nusselt number in the cooling regime.

The effectiveness of water-alumina nanofluid in comparison with the base fluid is studied by plotting the average heat transfer coefficient against the required pumping power. The nanofluid provides higher values of heat transfer coefficients than the base fluid in the considered range of pumping power with the increase of nanoparticle volume fraction. At the same time, the increase up to 1% and the decrease up to 4% of the heat transfer coefficient depending on Pe due to thermophoretic effect for the heating and cooling regimes, respectively, reveal that the water-alumina nanofluid is less effective under cooling than under heating. The present study shows that the influence of thermophoresis on heat transfer in the tube is rather weak since nanoparticle concentration varies only in the thin boundary layer near the tube wall.

The authors are grateful to Dr. A. V. Minakov for assistance in ANSYS Fluent numerical calculations. This work is supported the Krasnoyarsk Regional Foundation of Scientific and Technical Activity (Grant 02/13).

Nomenclature

r	radial coordinate (m)
z	axial coordinate (m)
R	tube radius (m)
L	heated section length (m)
u	radial velocity (m/s)
v	axial velocity (m/s)
v_0	average axial velocity (m/s)
$\boldsymbol{v}_T$	thermophoretic velocity (m/s)
T	temperature (K)
T_0	inlet temperature (K)
H	specific enthalpy (J/kg)
C_m	mass fraction of nanoparticles
C_v	volume fraction of nanoparticles
C_{m0}	inlet mass fraction of nanoparticles
C_{v0}	inlet volume fraction of nanoparticles
$\boldsymbol{\mathcal{J}}$	nanoparticle flux (kg/m^{2}s)
q	heat flux (W/mK)
ρ	density (kg/m^3)
ρ_0	reference density (kg/m^3)
β_T	thermal expansion coefficient (K^{-1})
μ	dynamic viscosity (Pa s)
κ	thermal conductivity (W/mK)
c_p	specific heat capacity (J/kg K)
χ	thermal diffusivity (m^2/s)
$\mathcal{D}$	diffusion coefficient (m^2/s)
$\mathcal{D}_T$	thermophoretic mobility (m^2/sK)
$\mathcal{S}_T$	Soret coefficient (K^{-1})
α	proportionality coefficient (kg m/s^2)
τ_w	wall shear stress (Pa)
h	heat transfer coefficient (W/m^2 K)
$\overline{h}$	average heat transfer coefficient (W/m^2 K)
W_p	pumping power (W)
Q	volume flow rate (m^3/s)
k_B	Boltzmann's constant (J/K)
d_a	nanoparticle diameter (m)
Π	viscous stress tensor (Pa)
E	unit tensor
ξ	dimensionless axial coordinate
Re	Reynolds number
Pe	thermal Peclet number
Pe$_c$	solutal Peclet number
Nu	Nusselt number
$\overline{\text{Nu}}$	average Nusselt number

Superscripts	
T	transpose

Subscripts	
b	bulk
w	water
a	alumnia nanoparticles
f	fluid
p	particle

References

1. S.K. Das, S.U.S. Choi, W. Yu, T. Pradeep, *Nanofluids: science and technology* (Wiley-Interscience Hoboken, 2008).
2. W. Yu, D.M. France, E.V. Timofeeva, D. Singh, J.L. Routbort, Appl. Phys. Lett. **96**, 213109 (2010).
3. S.U.S. Choi, J. Heat Transfer **131**, 033106 (2009).
4. X.Q. Wang, A.S. Mujumdar, Int. J. Thermal Sci. **46**, 1 (2007).
5. J.A. Eastman, S.R. Phillpot, S.U.S. Choi, P. Keblinsky, Annu. Rev. Mater. Res. **34**, 219 (2004).
6. M. Chandrasekar, S. Suresh, Heat Transfer Engin. **30**, 1136 (2009).
7. V.I. Terekhov, S.V. Kalinina, V.V. Lemanov, Thermophys. Aeromech. **17**, 1 (2010).
8. J. Buongiorno, ASME J. Heat Transfer **128**, 240 (2006).
9. W.H. Yu, D.M. France, J.L. Routbort, S.U.S. Choi, Heat Transfer Engin. **29**, 432 (2008).
10. V.I. Terekhov, S.V. Kalinina, V.V. Lemanov, Thermophy. Aeromech. **17**, 157 (2010).
11. Y. Ding, H. Alias, D. Wen, R. Williams, Int. J. Heat Mass Transfer **49**, 240 (2006).
12. U. Rea, T. McKrell, L. Hu, J. Buongiorno, Int. J. Heat Mass Transfer **52**, 2042 (2009).
13. W. Williams, J. Buongiorno, L.W. Hu, J. Heat Transfer **130**, 042412 (2008).
14. A.T. Utomo, E.B. Haghighi, A.I.T. Zavareh, M. Ghanbarpourgeravi, H. Poth, R. Khodabandeh, B. Palm, A.W. Pacek, Int. J. Heat Mass Transfer **69**, 77 (2014).
15. A.V. Minakov, A.S. Lobasov, M.I. Pryazhnikov, D.V. Guzei, Defect Diffusion Forum **348**, 123 (2014).
16. D. V. Guzei, A. V. Minakov, V. Ya. Rudyak, A. A. Dekterev, Tech. Phys. Lett. **40**, 203 (2014).
17. D. Wen, Y. Ding, Int. J. Heat Mass Transfer **47**, 5181 (2004).
18. K.S. Hwang, S.P. Jang, S.U.S. Choi, Int. J. Heat Mass Transfer **52**, 193 (2009).
19. Y. Xuan, Q. Li, ASME J. Heat Transfer **125**, 151 (2003).
20. V. Bianco, O. Manca, S. Nardini, Adv. Mech. Engin. **2010**, 976254 (2010).
21. D. Wen, Y. Ding, Microfluid Nanofluid **1**, 183 (2005).
22. D. Wen, L. Zhang, Y. He, Heat Mass Transfer **45**, 1061 (2009).
23. C.H. Sohn, K.D. Kihm, J. Korean Phys. Soc. **55**, 2200 (2009).

24. Y.S. Na, K.D. Kihm, J.S. Lee, Appl. Phys. Lett. **101**, 083111 (2012).
25. Y.S. Na, K.D. Kihm, J.S. Lee, Int. J. Heat Mass Transfer **55**, 7933 (2012).
26. M. Bahiraei, S.M. Hosseinalipour, Thermochim. Acta **574**, 47 (2013).
27. M.M. Heyhat, F. Kowsary, ASME J. Heat Transfer **132**, 062401 (2010).
28. I.I. Ryzhkov, Int. J. Heat Mass Transfer **66**, 461 (2013).
29. P.S. Epstein, Z. Physik. **54**, 537 (1929).
30. G.S. McNab, A. Meisen, J. Colloid Interface Sci. **44**, 339 (1973).
31. R. Piazza, A. Parola, J. Phys. Condens. Matter **20**, 153102 (2008).
32. A. Würger, Rep. Prog. Phys. **73**, 126601 (2010).
33. G. Galliero, J. Chem. Phys. **128**, 064505 (2008).
34. I.I. Ryzhkov, A.V. Minakov, Int. J. Heat Mass Transfer **77**, 956 (2014).
35. NIST Chemistry Webbook (2011).
36. R. Morrell, *Handbook of properties of technical and egineering ceramics*, *Part 2. Data reviews. Section 1. High-alumina ceramics* (London, 1987).
37. W.D. Kingery, H.K. Bowen, D.R. Uhlmann, *Introduction to Ceramics*, 2nd edition (John Wiley & Sons, New York, 1976).
38. A. Einstein, Ann. Phys. **19**, 289 (1906).
39. S. Iacopini, R. Rusconi, R. Piazza, Eur. Phys. J. E. **19**, 59 (2006).
40. M. Braibanti, D. Viglio, R. Piazza, Phys. Rev. Lett. **100**, 108303 (2008).
41. J.C. Giddings, P.M. Shinudu, S.N. Semenov, J. Colloid Interface Sci. **176**, 454 (1995).
42. J. Lenglet, A. Bourdon, J.C. Bacri, G. Demouchy, Phys. Rev. E. **65**, 031408 (2002).
43. S. Alves, F.L.S. Cuppo, A. Bourdon, A.M.F. Neto, J. Opt. Soc. Am. B. **23**, 2328 (2006).
44. J.H. Lienhard, J.H. Lienhard IV, *A heat transfer textbook* (Dover publications, New York, 2011).